

Refined scenario of the collinear cluster tri-partition mode with the greatest yield

Yu. V. Pyatkov^{1,2}, D. V. Kamanin², Yu. M. Tchuvil'sky³, A. A. Alexandrov², I. A. Alexandrova²,
Z. I. Goryainova², V. Malaza⁴, E. A. Kuznetsova², A. O. Strekalovsky², O. V. Strekalovsky^{5,2},
Sh. Wingaard⁶, and V. E. Zhuchko²

¹*National Nuclear Research University MEPhI (Moscow Engineering Physics Institute), Moscow, Russia*

²*Joint Institute for Nuclear Research, Dubna, Russia*

³*Skobeltsyn Institute of Nuclear Physics, Lomonosov Moscow State University, 119991 Moscow, Russia*

⁴*University of Stellenbosch, Faculty of Military Science, Military Academy, Saldanha 7395, South Africa*

⁵*Dubna State University, 141980 Dubna, Russia*

⁶*University of Stellenbosch, Stellenbosch, Western Cape, South Africa*

Background In our previous publications we discussed various manifestations of a new decay channel of the low excited heavy nuclei called collinear cluster tri-partition (CCT). The most populated CCT mode was revealed in the mass correlation distribution of fission fragments (FFs) as a local region ("bump") of increased yields below the loci linked to the conventional binary fission. The bump was dubbed "Ni-bump" because it is centered at the masses associated with the magic isotopes of Ni. Intriguing features of the CCT, especially high collinearity of the CCT partners and relatively high probability comparable with that typical for conventional ternary fission, have caused rather wide discussion. In the majority of dedicated publications, the FFs partitions from the Ni-bump have been analyzed from the different points of view. In our publications, we have underlined that Ni-bump manifests itself at the detectable level only in the spectrometer arm that faces the source backing. So far, this fact has been left beyond the scope of all known theoretical considerations, while the backing likely plays a crucial role in the observation of the CCT experimental pattern.

Purpose: To present new experimental data confirming the main features of the Ni-bump. To refine the CCT scenario and parameters of the process.

Method: Only two out of three CCT partners were detected in the experiment discussed here, and missing mass served as a sign of ternary decay. Recently we have modified hardware and software used in this experimental approach. Fast digitizer allowed to obtain digital images of the signals from all detectors. The data were processed off-line using numerical methods which are more robust with respect to the variety of signal shapes in comparison to the algorithms implemented in the CAMAC modules used by us previously.

Results: New experimental data obtained with three times larger statistics as in our previous experiments confirm the structure peculiarities of the Ni-bump. For the first time, a specific rhombic-like structure consisting of the lines corresponding to the fixed missing mass and the lines approximately perpendicular to them was revealed in the FFs mass correlation distribution. Each of the vertexes of the structure coincides with the masses of two magic nuclei. In the previous experiments, we observed only several separate fragments of this structure.

A range of the qualitative models proposed in this work are aimed to refine the mechanisms behind the second rupture of the intermediate fragment formed after the first rupture and a collinearity of the CCT partners.

Conclusions: In the frame of the essentially modified experimental method, the linear structures in the FFs mass correlation distribution were reproduced. The lines corresponding to the relations $M_1 = \text{const}$, $M_2 = \text{const}$, $M_1 + M_2 = \text{const}$ and $M_1 - M_2 = \text{const}$ for the masses M_1 and M_2 of the FFs detected in the opposite spectrometer arms form both the rectangular-like (Ni-bump) and the rhombic-like configurations with the vertices corresponding to the magic nuclei. The structures are statistically reliable, they are conditioned by a pronounced and complex correlation between the masses of the FFs measured independently. Such correlation seems to be a strong additional proof of a non-random nature of the structures observed.

In this work, we propose a self-consistent qualitative model of the Ni-bump. We suppose that the CCT mode manifesting as the Ni-bump is a two stages sequential decay process of the very deformed initial state. The shape and deformation energy of the intermediate Cd-like fragment formed after the first rupture allows to populate the shape isomer state of this nucleus. The passage of the intermediate fragment through the backing of the Cf source provides an alignment of the well

elongated nucleus with its linear momentum causing the collinearity of all three decay partners after the second rupture. Coulomb inelastic scattering of the intermediate fragment being in the shape isomer state leads to its break-up.

PACS: 23.70.+j–Heavy-particle decay; 25.85.Ca–Spontaneous fission;

I. INTRODUCTION

In our basic publications dedicated to collinear cluster tri-partition (CCT) [1–3] of heavy low excited nuclei, we have presented multiple experimental indications of this new type of multibody decay. In the most recent paper [4], we have discussed the physical scenario behind the so-called “Ni-bump”. This most populated CCT mode manifests itself in the mass correlation distribution of fission fragments (FFs), mainly via linear structures $M = \text{const}$, with the constants corresponding to the masses of the magic nuclei of $^{68,72}\text{Ni}$ and ^{128}Sn . After or almost simultaneously with our paper [4] several theoretical works dedicated or related to the CCT were published.

In Ref. [5] the limits imposed by quantum mechanical principles on angular distribution of a tri-partition process were obtained. The authors came to the conclusion that only the sequential and “almost sequential” mechanisms may result in quasi-collinear events, but in any case, the estimated lower limit of the width of the angular distribution for the light (“Ni-like”) CCT partner exceeds experimental value. Nevertheless, the limit obtained in Ref. [5] is much less pessimistic when compared to that from Ref. [6]. Very specific argument in favor of the CCT channel in ^{238}U was found in Ref. [5] using the geochemical data. Abnormal abundance of ^{38}Ar in various samples of the uranium ore is agreed with that typical for the CCT by the yield.

Ternary fission of ^{252}Cf was studied in Ref. [7] using three-cluster and unified ternary fission models based on classical physics concepts. Collinear and equatorial pre-scission configurations were analyzed in ternary fission with the ^{10}Li as the third fragment. For the fragment combination showing the highest relative yield both models predict collinear configuration.

Scission point model was applied in Ref. [8] for the mass distribution of ternary fission in ^{235}U (n_{th} , f) reaction. The obtained results indicate that the CCT mode associated with double closed shell ^{132}Sn is achievable if the process of ternary fission happens in two stages: i) formation of ^{132}Sn plus elongated partner; ii) subsequent breaking of the elongated partner into another closed shell nucleus ^{48}Ca and the remaining fragment of ^{56}Ti .

The trajectory calculations carried out in Ref. [9] allowed to numerically estimating the kinetic energy and position of different ternary fission fragments and the set of initial parameters including the initial emission angle of ternary particle. The initial angle is measured with respect to the axis connecting the centers of the side heavy fragments. The authors note: “As the size of the third fragment increases, the orthogonal and/or equatorial type emission is found to vary as the initial angle varies. In particular, for the lowest initial angle of 1° considered for the present study, the trajectory is found to be collinear supporting the experimental claims of collinear cluster tripartition.”

True ternary fission of ^{252}Cf was a subject of critical examination by means of the trajectory calculations in Ref. [10]. The authors calculated angular distribution of the fragments with the aim to study the effect of the spins of the fragments arising at the moment of scission. Both scissions were assumed to occur nearly simultaneously as opposed to our experimental findings. The total spin is compensated by the orbital angular momentum of the relative motion of the fragments. The orbital momentum gives evidence of the initial velocities of the FFs which are perpendicular to the fission axis. The fragments are supposed to stay collinear on a rotating fission axis. This assumption is not obvious for the ternary system but just the allowance for the initial transverse velocity results in the final angular divergence of the fragments. The predicted angular divergence of the CCT partners is very low and does not exceed one degree at reasonable initial conditions.

For the first time, the study of the excitation energy-dependent potential-energy surfaces for both the spherical and deformed fragments from the ternary fragmentation of ^{252}Cf at four different excitation energies of the fissioning nuclei was performed in Ref. [11]. For the spherical fragments, some energy maxima were obtained around magic and/or semi-magic numbers of nuclei. Calculations for deformed ternary fragments showed the energy maximum around the charge numbers of the fragments $Z_3 = 16$ with $Z_2 = 38\text{--}34$ and $Z_1 = 44\text{--}48$ region due to the presence of higher β_2 deformation values

We would like to refer to the work [12] from the related field of physics. The resonance scattering of diatomic molecules (dimers) by

atoms via three-particle metastable trimer states and the molecular dissociation induced by collisions with atoms were considered. Accuracy to potential replacement, the developed approach could be useful for analysis of interaction of the CCT-born di-nuclear systems when they pass through the source backing. The authors of work [12] also mention the CCT as a field of application of the developed methods.

As emphasized in our publications [1, 2], we have only observed the Ni-bump in the spectrometer arm facing the Cf source backing. So far, this peculiarity was beyond the scope of the theoretical considerations, but it plays likely a decisive role in observing the effect, as will be demonstrated below. Another motivation for this paper is to present our new experimental results obtained recently.

II. EXPERIMENTS

Most of our experiments in recent years were dedicated to searching for the rare decay modes of

low excited actinide nuclei while paying special attention to reliability of identification of such fission events. To increase the reliability the shapes of the signals have digitized with off-line processing of the signal images. Here we present the results of the experiment (Ex1) performed using such data processing approach. The scheme of the setup is shown in Fig. 1. It is the double-armed time-of-flight spectrometer of fission fragments (FFs). Two “start” timing detectors on the microchannel plates *St1* and *St2* were placed in the center of a vacuum chamber with a ^{252}Cf (sf) source on a $50\text{ }\mu\text{g}/\text{cm}^2$ thick Al_2O_3 backing between them. In the timing detector the fragment passes through a $32\text{ }\mu\text{g}/\text{cm}^2$ thick Lexan foil with a $40\text{ }\mu\text{g}/\text{cm}^2$ thick gold layer on it. Four mosaics of eight PIN diodes each provided measurement of both the FF energy and time-of-flight. The mean flight-pass for each mosaic did not exceed 15 cm and the working area of the PIN diode was $1.8\times 1.8\text{ cm}^2$.

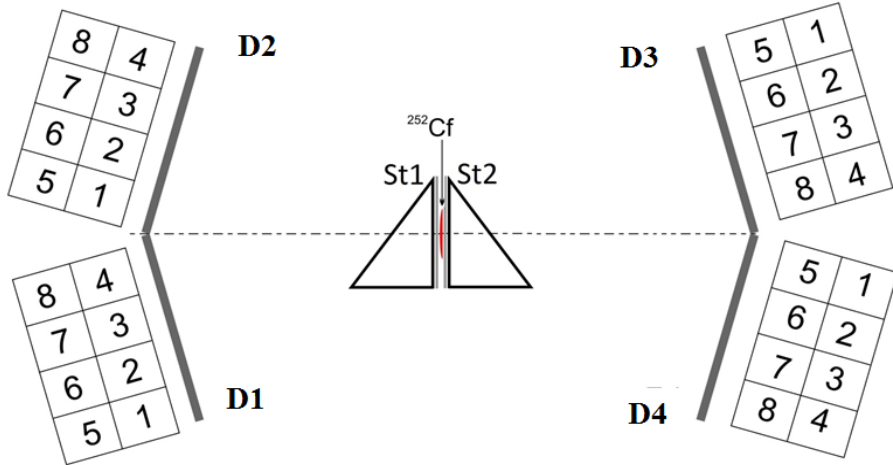


FIG. 1. Ex1: layout of the experimental setup. The ^{252}Cf (sf) source is placed between two “start” timing detectors on the microchannel plates *St1* and *St2*. Four mosaics (*D1*÷*D4*) of eight PIN diodes each provide measuring of both the FF energy and time-of-flight. The mean flight-pass for each mosaic does not exceed 15 cm and the working area of the PIN diode is $1.8\times 1.8\text{ cm}^2$.

The data acquisition system consisted of the multichannel fast flash-ADC (Amplitude to Digital Converter) digitizer CAEN DT574, logic blocks providing trigger signals, and a personal computer. Current value of the signal was measured by the digitizer every 0.2 ns.

Time reference point on the PIN diode signal was calculated using new algorithm proposed earlier [13]. The algorithm fits the initial part of a leading edge of the PIN diode signal with parabola function, under condition that the parabola vertex lays on the mean value of the signal’s base line. The parameters of the function are calculated using χ^2 minimization of several

points at the leading edge above three sigma (standard deviation of the base line values) level. Experimental testing at accelerator beam proved that this method gives unbiased, “true”, time reference corresponding to the real start of the signal [13]. Thus, skewness of the time-of-flight due to so called “plasma delay” (PD) [14] is eliminated.

Calculation of the FF mass with accounting for pulse-height-defect (PHD) was performed in iterative procedure based on parametrization proposed in Ref. [15]. The calculation algorithm was presented in Ref. [16].

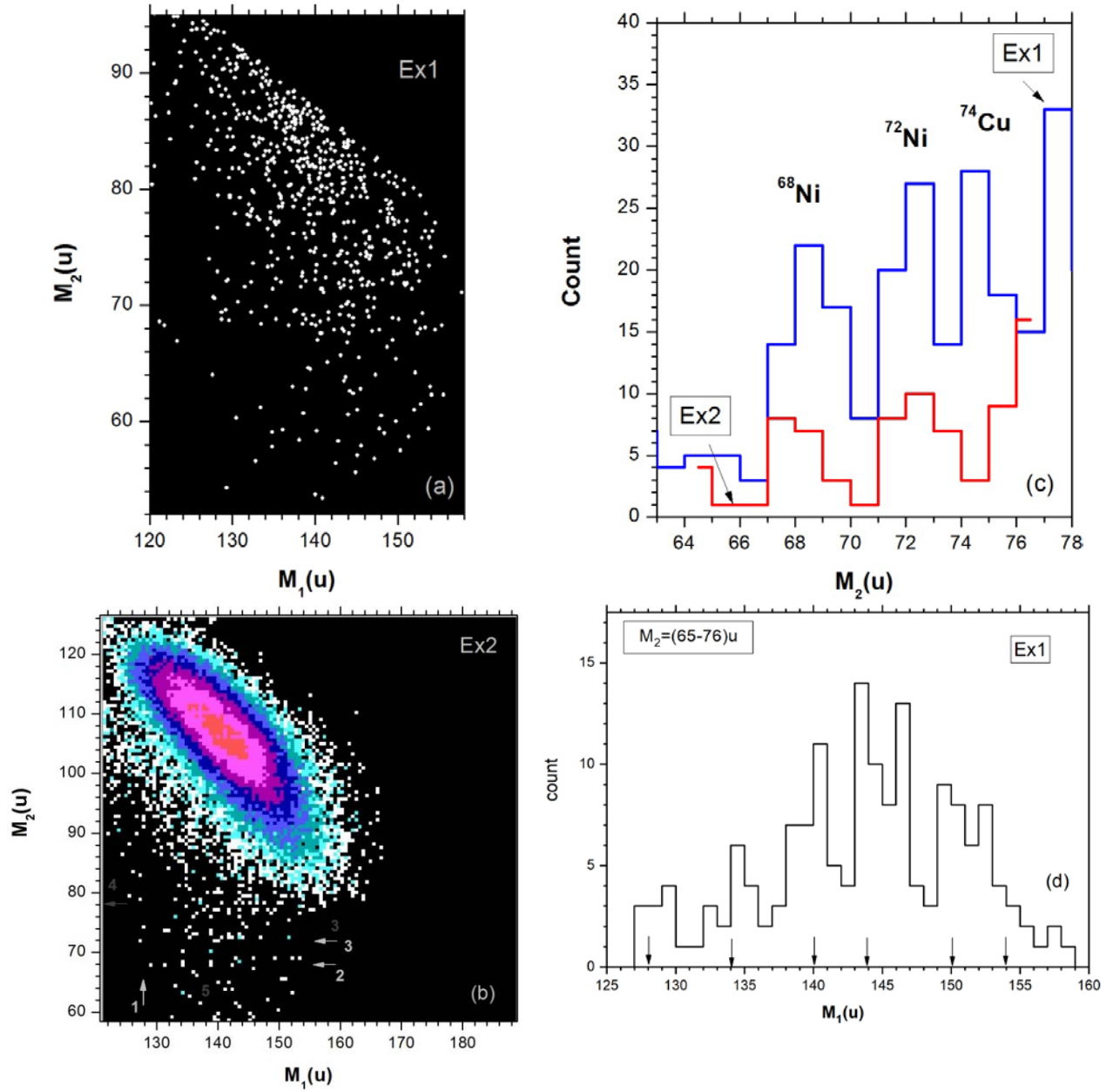


FIG. 2. (Color online). FFs mass correlation distributions from $^{252}\text{Cf(sf)}$ obtained in Ex1 – (a) and Ex2 – (b). Comparison of their projections onto M_2 axis – (c), projection of the distribution onto M_1 axis under condition that $M_2 = (65-76)u$ – (d). Positions of the magic nuclei are marked by the arrows. It should be noted that (b) was published in Ref. [2]. See text for the details.

Below the results of Ex1 will be compared with those obtained earlier in Ex2. This experiment was described in detail in our previous publications [2, 4]. The setup used in Ex1 had larger aperture (four mosaics of PIN diodes instead of two), different electronics and data processing procedures compared to Ex2. Flash-ADC and CAMAC modules provided data acquisition in Ex1 and Ex2, respectively. The FF mass reconstruction procedure in Ex1 was based on a direct accounting for both PD and PHD while interpolation of their influence in the energy range from alpha-particles up to FFs was utilized in Ex2 [2].

III. RESULTS

FFs mass correlation distribution in the region of the “Ni-bump” [2] obtained in Ex1 is presented in Fig. 2(a). Due to the actual background conditions, the events with the energy of the light fragment in the range $E_2 = (6 \div 30)$ MeV were selected. Similar distribution from Ex2 is shown in Fig. 2(b). The projections of the mass correlation distributions onto M_2 axis are compared in Fig. 2(c). As can be inferred from the Fig. 2(c), the statistics in Ex1 are approximately three times more than that in Ex2. A total yield of two Ni peaks in Ex1 does not exceed 2×10^{-4} per binary fission what agrees with previously

obtained value. The data of Ex2 indicated that the heavy clusters in the ternary pre-scission configurations are predominantly magic nuclei as it was supposed in Ref. [4] (see Table 1 in work [4]). Noticeably large statistics in Ex1 allowed confirming this assumption. The projection of the distribution shown in Fig. 2(a) onto M_1 axis for the range of $M_2 = (65-76)$ u (Fig. 2(d)) vividly demonstrates increased yield of the heavy fragments, corresponding to the magic isotopes of ^{128}Sn , ^{134}Te , ^{140}Xe , ^{144}Ba , ^{150}Ce , ^{154}Nd (their masses are marked in Fig. 2(d) by the arrows).

The data from Ex1 along with the presence of the lines at the mass numbers $A = 128, 68, 72$ (Fig. 2(a)) similar to those observed in Ex2 (marked by the numbers 1, 2, 3 respectively in Fig. 2(b)), show some additional structure. It consists of the family of lines $M_1 + M_2 \approx \text{const}$ at an angle of 45° to x -axis (partially presented in Ex2 as well) and some lines almost perpendicular to them. This rhombic-like structure will be discussed in our forthcoming paper.

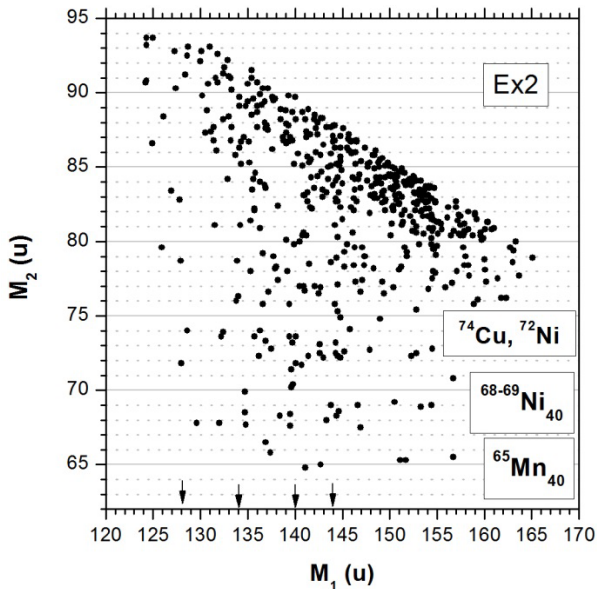


FIG. 3. Demonstration of the “fine structure” of the “Ni-bump”: mass correlation distribution observed in Ex2 with less statistics compared to Fig. 2(b). See text for details.

We have paid special attention to the additional peak centered at the mass $M_2 = 74$ u in Ex1 data (Fig. 2(c)). The origin of the peak becomes clear from the analysis of the mass correlation distribution obtained in Ex2 (Fig. 3), with less statistics compared to Fig. 2(b). Fig. 3 demonstrates the “fine structure” of the “Ni-bump”. Line $M_2 = 68$ u, associated with isotope of $^{68}\text{Ni}_{40}$, starts at $M_1 = 128$ u (presumably ^{128}Sn) and continues to mass $M_1 = 144$ u (magic isotope of ^{144}Ba). Then the line switches to the mass $M_2 = 69$ u likely corresponds also to isotope of Ni. Thus, magic proton shell $Z = 28$ and neutron

subshell $N = 40$ provides the effect. The next structure starts at the point $(134, 70)$ u and then transforms into the line $M_2 = 65$ u. According to the unchanged charge density hypothesis (UCD hypothesis) $N = 40$ corresponds to $Z = 25$ thus the horizontal line is due to the isotope of $^{65}\text{Mn}_{40}$. One more structure lies above the structures discussed above. The horizontal line starts at the point $(128, 74)$ u and continues to mass $M_1 \approx 140$ u (magic isotope of ^{140}Xe) and “jumps” to the mass $M_2 = 72$ u. In the frame of the UCD hypothesis, the masses $M_2 = 74, 72$ u are associated with ^{74}Cu and ^{72}Ni nuclei respectively.

IV. DISCUSSION

A. Population of the shape isomer state in the intermediate fragment.

The analysis of the energies of the FFs linked to Ni-bump allowed us to come to conclusion that the first rupture occurs in a very elongated configuration of the decaying system [4]. Calculations of the potential energy surface of the ^{252}Cf nucleus [17] performed using the Strutinsky prescription showed that at large deformations of the nucleus there are two distinct potential valleys. In both valleys, after the rupture, at the narrowest section of the neck, almost all the deformation energy concentrates in the heavy or light fragment respectively (Figs. 4(a), 4(b)). Such asymmetric partition of the deformation energy is confirmed by the neutron data [18]. Recent calculations of the potential energy surfaces for some super-heavy nuclei [19] applying the same theoretical approach showed similar shapes of the fissioning system near scission point. The result for the ^{280}Ds nucleus is presented in Fig. 4(c).

As it was mentioned in Ref. [20]: “Scission configuration has one almost spherical fragment with $A_L \approx 136$ and one extremely deformed (neck shaped) complementary fragment. After rupture of the first neck (with smallest radius), the light spherical fragment is separated from the rest. The question is: will the heavy deformed fragment undergo a second fission or will it recover a more or less compact shape? *In other words: is the fission of super-heavy elements (SHE) binary or sequential-ternary?*” At present, there is no published answer to this question for the SHE but it can be proposed for the ^{252}Cf nucleus.

Similar to the ternary mass split $^{72}\text{Ni}-^{52}\text{Ca}-^{128}\text{Sn}$ at the left boundary of the Ni-bump (Figs. 2(a), 2(b)), the CCT fragments will be dubbed “Ni-like”, “Ca-like” and “Sn-like”. The light fragment formed after the first rupture (*intermediate fragment*) will be dubbed “Cd-like” nucleus.

The experimental data on the kinetic energies of the CCT partners indicate the sequential or semi sequential character of the process [4]. It means that there is a delay between the consecutive ruptures, at least comparable with the time of full acceleration of the Cd-like fragment, and at the same time this fragment is excited enough to undergo fission. Both requirements could be met if the Cd-like nucleus is formed *in the fission isomer state*. This hypothesis mentioned also in Ref. [5, 21] will be quantitatively analyzed below.

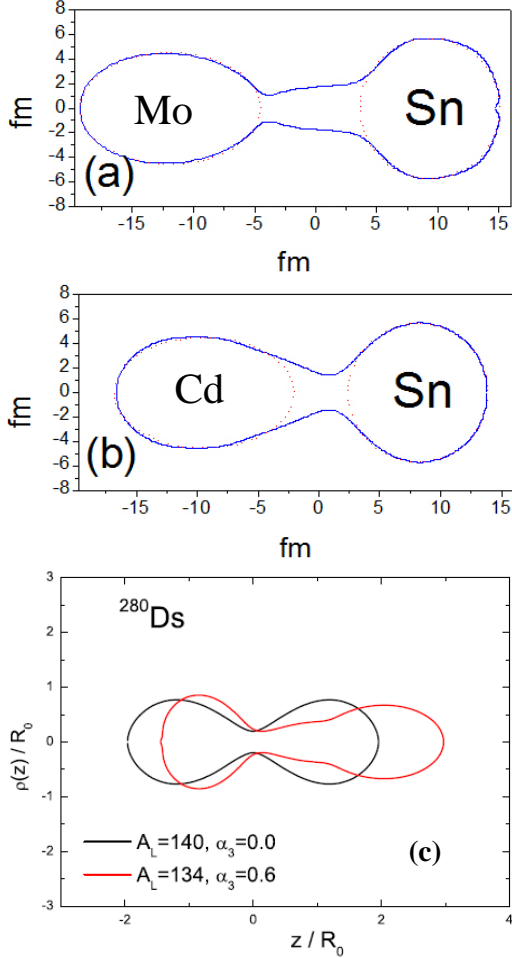


FIG. 4. The shapes of the ^{252}Cf nucleus for large elongations in two different potential energy valleys (a) and (b) [17]. The shapes of the super-heavy ^{280}Ds nucleus near the scission point for two values of the octupole deformation α_3 [19].

In both [4] and this work, the excitation energy $E_3^* \approx 30$ MeV of the FFs involved in the “Ni-bump” was estimated according to the formula:

$$E_3^* = Q_3 - \text{TKE}_3 \quad (1)$$

where Q_3 is a reaction heat of tri-partition, TKE_3 is a total kinetic energy of three fragments. Bearing in mind that Ni-like and Sn-like fragments are the magic nuclei (Fig. 2(b)), almost all E_3^* should be concentrated in the Ca-like fragment. At the same time, very elongated Cd-like fragment (Fig. 4(b))

formed after first scission could evolve to dumbbell-like shape that consists of the magic Ni-like and elongated Ca-like parts connected via well-defined neck, and E_2^* is mostly concentrated in the Ca-like nascent fragment (pre-fragment).

Similar shape is predicted, for instance, for the ^{232}Th nucleus at the third minimum of the fission barrier [22], Fig. 5. For the Cd nucleus discussed above, magic Ni and Ca nuclei could play the same role as magic Sn and Zr substructures in ^{232}Th .

Preformation of the nascent fragments at the top of the fission barrier, at least for the actinides, has been also confirmed in other theoretical approaches [23, 24].

Thus, it is reasonable to assume that $E_3^* \approx E_2^*$ because both values define the deformation energy of the same Ca-like fragment, or pre-fragment, in the ternary and binary fission respectively.

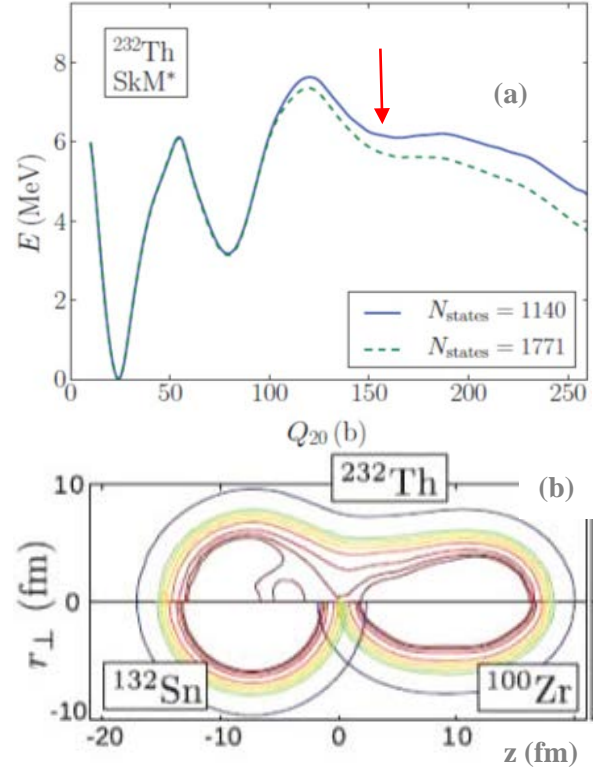


FIG. 5. (Color online) Potential-energy curve (fission barrier) for ^{232}Th calculated in the frame of the finite-temperature superfluid nuclear density functional theory [22] for two different numbers N of the basis states (a). Cross section of total density of ^{232}Th at third minimum ($Q_{20} = 165$ b) (b).

The value of E_2^* is very close to the fission barrier E_b of the Cd-like nuclei. For instance, for the isotope of ^{109}Cd the experimental value of E_b does not exceed 34 MeV (Table E in Ref. [25]). Experimental data from [26, 27] show that the barriers are peaked at symmetry and decrease towards both larger and smaller values of the mass

asymmetry. For the CCT events under discussion the mass asymmetry for the different partitions of the Ni/(Ca-like) fragments varies between $0.66 \div 0.36$, and this corresponds up to 10 MeV decrease of the fission barrier, for instance, for isotopes of Mo [27]. Therefore, population of the fission isomer state in the Cd-like fragment is not prohibited energetically.

B. Shape isomer state of the intermediate fragment: competition of fission and de-excitation.

In principal, there are three different ways of the system de-excitation from the shape isomer state. The first one could be tunneling of the system into the first well with the subsequent neutron and gamma-emission. Fission due to tunneling through the external barrier is also possible. The Coulomb induced break-up (induced fission) may occur, while the Cd-like fragment passes through the source backing.

The total probability of the break-up of the shape isomer state can be estimated as follows. At first it is necessary to refine the “true” yield of the events in the Ni-bump $Y(\text{Ni})$ comparing to all fission events detected. The experimental value of the yield $Y_{\text{exp}}(\text{Ni}) = 2 \cdot 10^{-4}$ per binary fission should be regarded as a lower limit of the yield. Peculiarities of the detection of almost collinear fragments with PIN diodes were examined in Ref. [2]. If Ni and Ca-like fragments are produced perfectly collinearly after the break-up of the Cd-like fragment, they are dispersed in the source backing in a fork-like manner with an opening angle $\theta_{\min} \approx 0.3^\circ$. Another limit $\theta_{\max} \approx 1^\circ$ is determined by the condition of the detection of the fork in the neighboring PIN diodes. The angle θ defines “the active area” along the PIN diode boundaries where one partner of the fork will be detected while the other one will be lost in the detector frame. Given this range of angles and actual dimensions of the setup (Fig. 1), $Y(\text{Ni}) = 4 \cdot 10^{-4} \div 1.2 \cdot 10^{-3}$.

The CCT doorway-state leading to the emission of the Ni isotopes (Fig. 2) is presumably elongated pre-scission configuration with very deformed Cd-like pre-fragment. Binary fission of such configuration manifests itself via asymmetry in the neutron multiplicity of the light and heavy fragments ν_L/ν_H : all neutrons are emitted from the Cd-like fragment, while the heavy one shows zero neutron multiplicity. The excitation energy of the Cd-like fragment is enough ($E_2^* \approx 30$ MeV) for emission of four neutrons, that agrees with the result obtained at the modified FOBOS setup [4]. The yields

$$Y(\nu = 4) = 30\% \text{ and}$$

$$[Y(\nu_L/\nu_H = 4/0)/Y(\nu = 4)] = 5.13\%,$$

where $Y(\nu = 4)$ – the yield of fission events with emission of four neutrons; $Y(\nu_L/\nu_H = 4/0)$ – portion of such events when all four neutrons are emitted from the heavy fragment. The yields above are known from the neutron data [28, 29]. Therefore the yield $Y(4/0)$ is estimated to be $1.54 \cdot 10^{-2}$. Taking into account the $Y(\text{Ni})$ range, the ratio $Y(\text{Ni})/Y(4/0)$ determining the probability of the break-up of the Cd-like nucleus in the source backing lies in the range of $3 \div 10\%$.

C. Alignment and break-up of a highly deformed fission fragment during its passing through a source backing medium.

It was stressed previously [1÷3] that the Ni-bump and other structures are clearly observed only in the spectrometer arm facing the source backing. The trivial role of the backing medium consists in deceleration of the fragment which energy losses exceeds some MeV. There exist, however, several more subtle effects.

Some of these effects could result in the alignment of the dipole moment of the fragment along its linear momentum direction. As an example, let us consider the form of an ion decelerated in a medium. The Coulomb interaction of the external electron shells of the ion with the medium is known to be the dominant factor of the energy losses at deceleration of the ion with the energy approximately 1 MeV/A typical for the fission fragments. At rest or when moving in vacuum a nucleus is located in the charge center of the electron shell of an atom or an ion. At deceleration, due to the inertia, the nucleus turns out to be shifted forward from the charge center of the electron shell. Thus, the nucleus is brought into a nonzero electric field directed anti parallel to the decelerating force.

As demonstrated above, the Cd-like intermediate nucleus in some cases is generated in fission process in the shape isomer state. This state looks like a di-nuclear system of Ni and Ca clusters. The shell effects make energetically preferable a certain difference in Z/A -ratios of the members of this pair. In this case the dipole moment of such a system appears. This dipole moment interacts with the nonzero electric field of the electron shell. This effect may align the axis of the di-nuclear system to be parallel to linear momentum of the ion. Other mechanisms of the in-medium alignment should also be subjects of such an analysis. In particular, we have in mind interaction of the large quadrupole moment of the discussed fragment with quadrupole moments of the source backing atoms.

All these mechanisms may be treated by analogy with stabilization mechanisms typical for ballistic problems. Any deviation of the symmetry axis of the prolate body from the direction of a decelerating force causes the restoring force to occur [30].

Another consequence of our experimental results is that we can confidently say that initially excited Cd-like fragment undergoes a break-up while passing source backing foil.

The idea of fission induced by Coulomb interaction was introduced more than fifty years ago [31]. Further improvement of the theoretical description of the Coulomb fission was performed in Refs. [32, 33]. Differential cross-section of about 50 mb/sr for the Coulomb fission of ^{238}U due to interaction with ^{148}Nd projectile at energy $E = 500$ MeV in the c. m. frame was predicted in Ref. [32]. In our case the masses, charges, shapes and energies of the interacting nuclei are substantially different. And what is particularly important, the state of the Cd-like nucleus formed by a Cf fission event is supposed to be in the second or the third well (in the case that the latter exists), as it has just been demonstrated (see for instance Fig. 5). The external barrier of such well is expected to be incomparably lower than the fission barriers of actinides in their ground states. Excited states of such a type could be referred to as shape isomer ones and according to [34] may be treated as di-nuclear systems. These states may be also considered as hyper-deformed ones [34-36], with the only difference that their angular momenta are not extremely large. The masses from the range $A = 105-130$ are considered to be promising for the search of hyper-deformed states [35]. Unfortunately, to date, the explicit form of the fission barriers of these nuclei is unknown. One more property of the Cd-like fragment is that due to its great elongation this nuclide possesses very small rotational quantum ($\hbar\omega \approx 1-2$ keV). Thus, the intensity of multi-step excitation of such objects during passing through a source backing medium is high and the probability to overcome the lower external barrier is expected to be high.

Mechanism of the Coulomb fission could be decisive for the alignment under discussion as well. Coulomb excitation is known [37] to result in a strong alignment of the symmetry axis of the fissioning nucleus perpendicular to the line connecting the center of mass of the target and projectile at the point of the closest approach where fission takes place. In the case under consideration, when the scattering angle of the Cd-like fragment is relatively small, similar orientation effect would provide an alignment of

the fragment and its linear momentum at the moment of scission.

It should be noted that all the considerations presented in this section are qualitative ones and therefore need further quantitative verification.

V. SUMMARY

The new experimental data with three time's larger statistics than before confirms the structure of the Ni-bump. Projection of the bump onto the axis of the light FFs masses shows the peaks centered at the mass numbers 68, 72, 74, associated with the magic isotopes of $^{68,72}\text{Ni}$ and ^{74}Cu (Fig. 2(c)). The projection onto the opposite axis also demonstrates the peaks at the masses, which could be assigned to the magic isotopes of ^{128}Sn , ^{134}Te , ^{140}Xe , ^{144}Ba , ^{150}Ce , ^{154}Nd [38]. The fine structure of the Ni-bump (Fig. 3) gives evidence that the bump exists due to the shell minima at $Z = 28-29$, and to the subshell $N = 40$.

The following scenario gives a self-consistent interpretation of the Ni-bump features observed. In this mode, the CCT occurs as a two stages sequential decay process of the very deformed pre-scission configuration (Fig. 4(b)). The shape and deformation energy of the intermediate Cd-like fragment formed after the first rupture allows to populate the shape isomer state of this nucleus in the second or third well at the top of the fission barrier. Thus, similar to the known fission isomers in actinides, the Cd nucleus in this state could be dubbed as *fission isomer of Cd*. It should be stressed that we observe *induced fission of Cd-like nucleus from the shape isomer state*. This nucleus (intermediate fragment) undergoes a Coulomb break-up while crossing the Cf source backing.

According to the scenario described above, only 3-10% of the prescission states of Cf nucleus with excitation of ≈ 30 MeV undergo the break-up.

The interaction of the intermediate fragment with the source backing is appeared to be also the origin of collinearity of the CCT partners.

ACKNOWLEDGMENTS

This work was supported, in part, by the Russian Science Foundation and fulfilled in the framework of MEPhI Academic Excellence Project (Contract No. 02.a03.21.0005, 27.08.2013), and by the Department of Science and Technology of the Republic of South Africa (RSA). We are grateful to R.V. Jolos, N.V. Antonenko, G.G. Adamian, V.I. Furman, A.K. Nasirov, N. Carjan for their continuous interest in the subject and the stimulating discussions.

- [1] Yu.V. Pyatkov, D.V. Kamanin, W. von Oertzen, A.A. Alexandrov, I.A. Alexandrova, O.V. Falomkina, N.A. Kondratjev, Yu.N. Kopatch, E.A. Kuznetsova, Yu.E. Lavrova, A.N. Tyukavkin, W. Trzaska, and V.E. Zhuchko, *Eur. Phys. J. A* **45**, 29 (2010).
- [2] Yu.V. Pyatkov, D.V. Kamanin, W. von Oertzen, A.A. Alexandrov, I.A. Alexandrova, O.V. Falomkina, N. Jacobs, N.A. Kondratjev, E.A. Kuznetsova, Yu.E. Lavrova, V. Malaza, Yu.V. Ryabov, O.V. Strekalovsky, A.N. Tyukavkin, and V.E. Zhuchko, *Eur. Phys. J. A* **48**, 94 (2012).
- [3] D.V. Kamanin and Yu.V. Pyatkov, in *Clusters in Nuclei*, Lecture Notes in Physics No. 875, edited by C. Beck (Springer, Berlin, 2013), Vol. 3, p. 183.
- [4] Yu.V. Pyatkov, D. V. Kamanin, A.A. Alexandrov, I.A. Alexandrova, Z.I. Goryainova, V. Malaza, N. Mkaza, E. A. Kuznetsova, A.O. Strekalovsky, O. V. Strekalovsky, and V. E. Zhuchko, *Phys. Rev. C* **96**, 064606 (2017).
- [5] T.V. Chuvil'skaya and Yu.M. Tchuvil'sky, *Phys. Rev. C* **99**, 024301 (2019).
- [6] P. Holmval, U. Köster, A. Heinz, and T. Nilsson, *Phys. Rev. C* **95**, 014602 (2017).
- [7] D. Naderi, A. Moradian, and M. Zargooshi, *Phys. At. Nucl.* **80**, 1073 (2017).
- [8] C. Karthika and M. Balasubramaniam, *Eur. Phys. J. A* **55**, 59 (2019).
- [9] K R Vijayaraghavan, V Gokula Lakshmi, P Prema and M Balasubramaniam, *J. Phys. G: Nucl. Part. Phys.* **46**, 025103 (2019).
- [10] F.F. Karpeshin, e-print arXiv: 1904.10598v1 [nucl-th], 24 Apr 2019.
- [11] C. Karthikraj and Zhongzhou Ren, *Phys. Rev. C* **101**, 014603 (2020).
- [12] A.A. Gusev, S.I. Vinitsky, O. Chuluunbaatar, A. Gózdź, V. L. Derbov, and P. M. Krassovitskiy, *Phys. At. Nucl.* **81**, 945 (2018).
- [13] D.V. Kamanin, Yu.V. Pyatkov, A.O. Strekalovsky, V.E. Zhuchko, Z.I. Goryainova, P.Yu. Naumov, A.A. Alexandrov, I.A. Alexandrova, N. Mkaza, E.A. Kuznetsova, V. Malaza, O.V. Strekalovsky, *Izvestiya Rossiiskoi Akademii Nauk. Seriya Fizicheskaya* **82**, 719 (2018).
- [14] H.O. Neidel and H. Henschel, *Nucl. Instrum. Methods* **178**, 137 (1980).
- [15] S.I. Mulgin, V.N. Okolovich, S.V. Zhdanov, *Nucl. Instrum. Methods Phys. Res. A* **388**, 254 (1997).
- [16] Yu.V. Pyatkov, D.V. Kamanin, N.A. Kondratjev, A.O. Strekalovsky, S. Ilić, A.A. Alexandrov, I.A. Alexandrova, N. Mkaza, E.A. Kuznetsova, V. Malaza, G.V. Mishinsky, O.V. Strekalovsky and V.E. Zhuchko, *J. Phys.: Conf. Ser.* **675**, 042018 (2016).
- [17] Yu.V. Pyatkov, V.V. Pashkevich, Yu.E. Penionzhkevich, V.G. Tishchenko, A.V. Unzhakova, H.-G. Ortlepp, P. Gippner, C.-M. Herbach, and W. Wagner, *Nucl. Phys. A* **624**, 140 (1997).
- [18] A.S. Vorobyev, V.N. Dushin, F.-J. Hambsch, V. A. Jakovlev, V. A. Kalinin, A. B. Laptev, B. F. Petrov, and O. A. Shcherbakov, *AIP Conference Proceedings* **798**, 255 (2005).
- [19] N.Carjan, F.A.Ivanyuk, Yu.Ts.Oganessian, *Nucl. Phys. A* **968**, 453 (2017).
- [20] N.Carjan, abstract of the laboratory seminar of FLNR (JINR), October 2, 2018.
- [21] D.V. Kamanin, Yu.V. Pyatkov, A.A. Alexandrov, I.A. Alexandrova, N.A. Kondratjev, E.A. Kuznetsova, V. Malaza, N. Mkaza, V.N. Shvetsov, A.O. Strekalovsky, O.V. Strekalovsky, V.E. Zhuchko, in Proceedings of the “22th International Seminar on Interaction of Neutrons with Nuclei”, Dubna, Russia, 27-30 May 2014, p. 70.
- [22] J. D. McDonnell, W. Nazarewicz, and J. A. Sheikh, *Phys. Rev C* **87**, 054327 (2013).
- [23] V. Pashkevich, Yu. Pyatkov, A. Unzhakova, in Proceedings of the “XV Workshop on Nuclear Physics “Marie and Pierre Curie”, Kazimierz Dolny, Poland, 24–28 September, 2008, p. 165.
- [24] Ken-ichiro Arita, Takatoshi Ichikawa, and Kenichi Matsuyanagi, *Phys. Rev. C* **98**, 064311 (2018).
- [25] P. Möller, J. Nix, W. Myers, and W. Swiatecki, *At. Data Nucl. Data Tables* **59**, 185 (1995).
- [26] D.N. Delis, Y. Blumenfeld, D.R. Bowman, N. Colonna, K. Hanold, K. Jing, M. Justice, J.C. Meng, G.F. Peaslee, G.J. Wozniak and L.G. Moretto, *Nucl. Phys. A* **534**, 403 (1991).
- [27] K.X. Jing, L.G. Moretto, A.C. Veeck, N. Colonna, I. Lhenry, K. Tso, K. Hanold, W. Skulski, Q. Sui, G.J. Wozniak, *Nucl. Phys. A* **645**, 203 (1999).
- [28] J.F. Wild, J. van Aarle, W. Westmeier, R.W. Loughheed, E.K. Hulet, K.J. Moody, R.J. Dougan, E.-A. Koop, R.E. Glaser, R. Brandt, and P. Patzelt, *Phys. Rev. C* **41**, 640 (1990).
- [29] A.S. Vorobyev, private communication and [18].
- [30] <https://www.grc.nasa.gov/www/k-12/rocket/shorttr.html>
- [31] L. Wilets and E. Guth and J.S.Tenn, *Phys. Rev.* **156**, 1349 (1967).
- [32] H. Holm and W. Greiner, *Phys. Rev. Lett.* **26**, 1647 (1971).
- [33] H.Kruse, W.T. Pinkston, and W. Greiner, *Phys. Rev. C* **22**, 2465 (1980).
- [34] G.G. Adamian, N.V. Antonenko, Z. Gagyipalfy, S.P. Ivanova, R.V. Jolos, Yu.V. Palchikov, W. Scheid, T.M. Shneidman, A.S. Zubov, in

Proceedings of the “Predeal International Summer School in Nuclear Physics” Predeal, Romania, 28 August–9 September 2006, p. 483.

[35] N. Schunck, J. Dudek, and B. Herskind Phys. Rev. C **75**, 054304 (2007).

[36] H. Abusara and A.V. Afanasjev Phys. Rev. C **79**, 024317 (2009).

[37] V.E. Oberackert, W.T. Pinkston, and H.G.W. Kruse, Rep. Prog. Phys., **48**, 327 (1985).

[38] J. Moreau, Licentiaatsthesis, R.U.G. (University of Gent), 1982